Turkish Journal of Civil Engineering, 2026, 47-76, Paper 831, ***Research Article***

Seismic Performance Improvement of a Reinforced Concrete Structure with Inter-Story Isolation

Furkan Yurdakul KAYIKÇI[1]
Ali GÜRBÜZ[2*]

ABSTRACT

This study investigates improving the seismic performance of a 6-story residential reinforced concrete building converted into a hospital using inter-story isolation. Lead rubber bearing was employed, with parameters optimized in accordance with the 2018 Turkey Building Earthquake Code for DD-1 and DD-2 earthquake ground motion levels. Three structural models were analyzed using nonlinear dynamic analysis, incorporating soil-structure interaction (SSI). Four earthquake records were scaled to DD-1 and DD-2 spectrum levels. Subsequently, 1D equivalent-linear site response analyses were conducted on these ground-motion records scaled to the design spectrum. The results demonstrate that inter-story isolation significantly enhances the seismic performance of the building, making it suitable for hospital use under seismic loadings.

Keywords: Reinforced concrete, inter-story isolation, soil- structure interaction, earthquake engineering, nonlinear time history analysis, finite element method.

1. INTRODUCTION

It is widely recognized that most existing buildings do not possess the necessary resistance to seismic forces. Managing structural seismic response has become a key research focus, aimed at enhancing seismic performance cost-effectively and efficiently. A substantial number of response control systems have been described in the literature, which can be classified into four principal categories: passive, active, semi-active and hybrid. In particular, base isolation systems, the first examples of which emerged in the 1970s, have demonstrated their efficacy and are now accepted in current earthquake codes [1]. While each system possesses distinctive advantages, certain constraints exist, including cost, noise, and the duration which the structure will be out of service during restoration of an existing structure.

Note:
- This paper was received on June 9, 2025 and accepted for publication by the Editorial Board on October 12, 2025.
- Discussions on this paper will be accepted by May 31, 2026.
- https://doi.org/10.18400/tjce.1716282

1 Recep Tayyip Erdoğan University, The Faculty of Engineering and Architecture, Rize, Türkiye
furkanyurdakul_kayikci24@erdogan.edu.tr - https://orcid.org/0000-0002-7399-5681

2 Recep Tayyip Erdoğan University, The Faculty of Engineering and Architecture, Rize, Türkiye
ali.gurbuz@erdogan.edu.tr - https://orcid.org/0000-0003-1123-9968

* Corresponding author

Inter-story isolation (ISI) is also used to enhance the earthquake performance of existing buildings. In general, seismic base isolation and inter-story isolation systems yield comparable results for low-rise buildings [2, 3]. Rather than incurring the financial burden of implementing seismic isolation at the foundation level of an existing structure, installing the isolation system one floor above offers a straightforward solution that does not significantly alter the outcome [4, 5]. For example, Topaloglu and Yanik [6] demonstrated through experimental studies on a five-story building that an ISI system can achieve results comparable to base isolation in limiting the lateral drift of the building.

If seismic damping systems are used, more sensitive analysis methods need to be applied [7]. Nonlinear dynamic analysis should be preferred to find the most realistic behavior of the structure and seismic damping systems [8, 9, 10]. Studies in the literature agree that soil-structure interaction (SSI) analyses provide more realistic results [11, 12, 13, 14]. To illustrate, Wan et al [11] conducted a seismic examination of a 10-story building constructed in a mountainous region with non-isolated floors, except for the 2nd and 3rd floors. The structure was subjected to seismic forces equivalent to the Kobe 1995 and El Centro 1949 earthquakes. The analysis of the structure, fixed to the ground, demonstrated that the structure withstood seismic loads (16 mm drift at the isolation level), yet the displacements of the isolator bearings considering soil-structure interaction exceeded the limit values (200 mm drift at the isolation), resulting in a reduction in acceleration. Xu et al [15] used inter-story isolation in a 6-story building and investigated the effect of SSI on the results. According to the results, when the SSI is considered, the natural period of the building increases by 1.2 times compared to the assumption of a rigid foundation.

In literature, many publications studying inter-story isolation in buildings considering soil-structure interaction have existed. Tsai et al [16] studied mid-story isolation in a structure which was modelled as a shear building. SSI was represented as lateral shear springs spread across multi-layered viscoelastic soil strata. The analyses were performed via closed form solutions in the frequency domain. Yingxiong et al [17] established 5-story structure on soft soil above shaking table and studied pile-soil and inter-story isolated building interaction. Dewen et al [18] established 5-DOF discrete system in order to study effect of inter-story isolation and analyzed together with near- field and far-field effects using Newmark method and SSI. Liu et al [19] modelled 18-story reinforced concrete building with C30-C40 concrete and HRB400 rebars in ETABS software. New staggered story isolation (base isolation + inter-story isolation) with 24 LRB500 and 12 LRB600 lead rubber bearings was used. SSI was represented as spring-damper and nonlinear time history analyses were performed via 3 real earthquake records from Nanjing, Tianjin and Lanzhou. Gao et al [20] modelled 12-story reinforced concrete frame building in SAP2000. Double-story isolated structure, mid-story isolated structure and base-fixed structure were compared to each other. Nonlinear time history elastoplastic analyses were performed via 3 earthquake records (Kern County, Whittier Narrows and Chi-Chi), and SSI was considered using ATC-40 and FEMA-440 methods. Topaloglu and Yanik [6] modelled 5-story reinforced concrete building in SAP2000 software. Lead rubber bearings were installed on both the base and mid-story of the structure, and SSI was represented by spring and damper elements. Nonlinear time history analyses were performed using Kocaeli (1999) and Loma Prieta (1989) earthquake records. Wan et al [11] modelled a 10-story reinforced concrete stilted building with C40 concrete in the down slope and transverse slope directions, and LRB800 and LRB900 isolators were used on the mid-story. SSI was represented by both traditional and variable parameters spring-

damper elements. Nonlinear time history analyses were performed using El Centro (1940) and Tangshan (1976) earthquake records. Wan et al [21] studied 9-story mid-story isolated reinforced concrete building with C40 concrete. Two different lead rubber bearings (LRB600, LRB800) and two different 3D isolators (3D LRB, T/C FPB) were used. SSI was represented by Mohr–Coulomb model and the soil was modelled as sloping ground. 1D, 2D and 3D nonlinear time history analyses were performed under 7 earthquake records. Xiao et al [22] studied seismic behavior of an 18-story mid-story isolated irregular reinforced concrete frame-core tube structure. Isolation layer was installed on 8th story, and LRB700, LRB800 and LRB900 were used. The structure was modelled in ETABS software and SSI was considered through multi-layered soil model. Nonlinear time history analyses were performed using 3 earthquake records from HEL, IPM and NWC. Xu et al [15] prepared a scaled steel model based on 8-story reinforced concrete structural prototype and used 4 lead rubber bearing for inter-story isolation. SSI was studied with rigid foundation and soft soil conditions. A silty clay filtered layered soil box was prepared. In the analyses, 12 earthquake records such as near-field/far-field ordinary, near-field pulse and far-field harmonic were used. Shaking table experiments were supported by finite element analyses. Yanık and Topaloğlu [23] modelled a 15-story reinforced concrete building in SAP2000 software. Three different model such as fixed-base model, base-isolated model and base- and mid-story isolated model were considered. Lead-rubber bearings were used as the isolator; the soil was modelled as medium-dense sand using the Winkler model. Nonlinear time history analyses were performed using the 1999 Kocaeli, 1995 Kobe, and 1989 Loma Prieta earthquakes. Wan et al [24] modelled a 10-story reinforced concrete building with C40 concrete. Lead-rubber bearings (LRB800 and LRB900) were used for mid-story isolation. SSI was modelled using finite element method on a soil layer with 300×180×30 m dimension and its elastic properties were defined. The soil was introduced by viscoelastic boundary conditions. A total of 10 earthquake records were used in the elastoplastic time history analyses (8 out of them were long-period and 2 out of them were ordinary). Yang et al [25] modelled a 65.3 m high reinforced concrete building with C40 concrete and studied mid-story isolated (in the 6th story) and double-story isolated (in the 6th and 11th stories) configurations. LRB600 lead-rubber bearing was used as isolator, and SSI was introduced by a spring model based on ATC-40 and FEMA440. A total of nine earthquake records (three out of them were normal and six out of them were far-field long period) were performed in three components, and elastoplastic time history analyses were performed.

This study aims to address the gap in practical knowledge regarding seismic resilience. The main goal is to improve the seismic performance of a six-story reinforced concrete building. This is achieved by integrating and optimizing the lead rubber bearing. A hypothetical scenario was developed for this research. According to this scenario, the goal is to convert a six-story residential reinforced concrete building into a hospital. As a result, the seismic resilience of the structure must be upgraded to meet the hospital construction standards outlined in local seismic regulations. To this end, inter-story isolation was added to the aforementioned building between the first and the second floor. To evaluate the structural performance, nonlinear time history analyses were performed using a 3D finite element model that incorporated both the soil and the structure, with four different ground-motion inputs scaled based on horizontal elastic design spectra. Then, these scaled earthquake ground-motion records were deconvoluted. The aim of incorporating SSI is able to show change in structural response due to arising from flexural deformation of the superstructure

founded on a flexible soil deposit. Finally, nonlinear time history analyses were conducted with reference to these deconvoluted ground-motion records. The analysis results were evaluated based on various factors such as maximum base shear force, floor accelerations, lateral displacements and inter-story drifts.

The novelty of this study is the optimization of the inter-story isolation system considering soil-structure interaction. Subsequently, the isolated buildings with optimized LRB were compared to the bare structure. Although several studies have examined inter-story isolation in building structures considering SSI, none have conducted the optimization of inter-story isolation under the effects of SSI. In addition, 1D equivalent-linear site response analyses were performed. This study aims to close this gap.

2. METHODOLOGY

In the models developed for analyzing the study scenario, soil-structure interaction was incorporated using a conventional method. A viscous boundary condition was applied to the interface between the near-field and the far-field. Nonlinear dynamic time-history analyses were performed on all these models. The columns and beams were represented using frame elements, while slabs and shear walls were modelled using shell elements. Soil was modelled using 8-noded solid elements. Isolation systems and boundary conditions were modelled using link elements. The structure itself is a framed reinforced concrete system resting on a raft foundation. The effective section stiffnesses for the columns, beams, shear walls, and slabs were determined according to [26] (Table 1). All systems were modelled using the finite

Table 1 - Effective section stiffness coefficients [26]

Reinforced concrete member	Effective section stiffness coefficient	
Shear wall-slab (In-plane)	Axial	Shear
Shear wall	0,75	1,00
Basement shear wall	1,00	1,00
Slab	0,50	0,80
Shear wall-slab (Out-of-plane)	Bending	Shear
Shear wall	1,00	1,00
Basement shear wall	1,00	1,00
Slab	0,50	1,00
Frame member	Bending	Shear
Grade beam	0,30	1,00
Frame beam	0,70	1,00
Frame column	0,90	1,00
Shear wall (equivalent frame)	0,80	1,00

element methods. Four earthquake records from the PEER database were used for the analyses [27]. These earthquake records were scaled to match both the DD-1 and DD-2 horizontal elastic design spectra. In international literature, DD-1 represents MCE (maximum credible earthquake) and DD-2 represents DBE (design basis earthquake). The lead rubber bearings were optimized based on both the analyzed building and the upper of lower bounds of DD-1 and DD-2. The isolation layer was positioned between the first floor and the second floor of the structure. In addition, the spectral matching, optimization of the lead rubber bearing, load combinations, analysis method, establishment of horizontal elastic design spectra used in this study and performance evaluation criteria were all carried out in accordance with [26]. Therefore, general analysis procedure of this study and performance evaluation were performed based on [26].

2.1. Soil-Structure Interaction and Viscous Boundary Condition

Analysis methods that consider the behavior of the soil provide more realistic results than analysis methods that assume the structure is fixed to the soil. However, the structure is built on an infinite soil medium. To analyze this infinite medium, it is necessary to constrain the soil at a point on the model. A viscous boundary condition is used to define the boundaries of the soil, which is modelled using a viscous damper link element [28, 29]. A schematic representation of the viscous boundary condition is shown in Figure 1 [30].

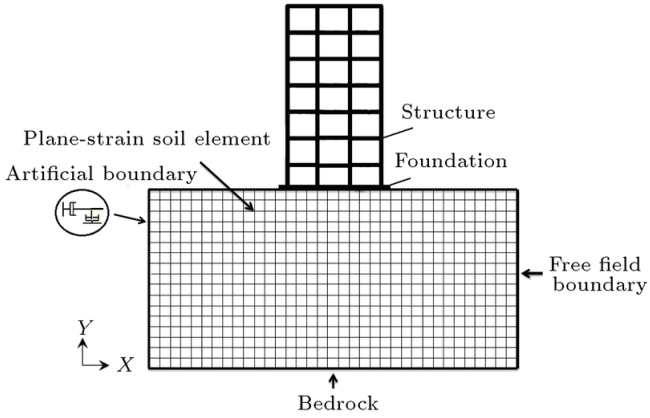

Figure 1 - Viscous boundary condition in soil-structure interaction [30].

When the viscous boundary condition is added to the soil boundary, the equation of motion of the system becomes as in Eq.(1) [31].

$$[M]\{\ddot{u}(t)\}+[C]\{\dot{u}(t)\}+[V]\{\dot{u}(t)\}+[K]\{u(t)\}=\{R(t)\} \quad (1)$$

In this equation, [M], [C] and [K] represent the mass, damping and stiffness matrices, respectively. {ü(t)}, {u̇(t)} and {u(t)} represent the acceleration, velocity and displacement

vector, respectively. {R(t)} represents the inertia force. The equations of the shear wave velocity and the pressure wave are obtained from Eq. (2) [26, 32, 33].

$$V_S = \sqrt{\frac{G}{\rho}},\ V_p = \frac{V_S}{s},\ s = \sqrt{\frac{1-2\upsilon}{2(1-\upsilon)}} \tag{2}$$

In Eq. (2), G represents the shear modulus, ρ denotes the unit volume mass of the soil, υ is the Poisson ratio of the soil, s is the elastic constant, V_S denotes the shear wave, and V_P is the compression wave. The effective damping and effective stiffness values for both shear wave and pressure wave are calculated using Eqs. (3)-(4).

For shear wave:

$$K_1 = K_2 = \frac{2G}{R}\sum_{i=1}^{I} A_i\,,\ C_1 = C_2 = \rho V_S \sum_{i=1}^{I} A_i \tag{3}$$

For pressure wave:

$$K_3 = \frac{4G}{R}\sum_{i=1}^{I} A_i\,,\ C_3 = \rho V_p \sum_{i=1}^{I} A_i \tag{4}$$

In these equations, K is the effective stiffness, C is the effective damping, R is the distance between the geometric center of the building and the boundary line of the soil. ΣA_i is the area represented by a node located on the artificial boundary [34]. To illustrate the viscous boundary condition, Figure 2 was presented.

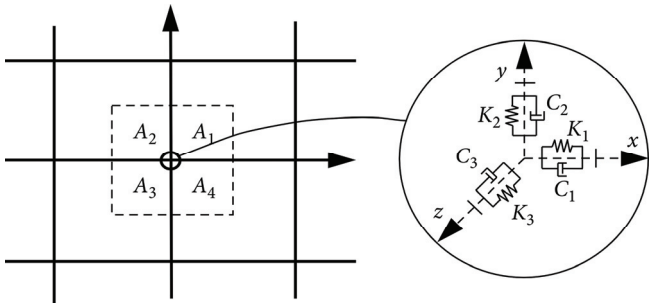

Figure 2 - Modelling of viscous-boundary condition [34].

2.2. Site Response Analysis

In this study, site response analysis was performed as follows: First, strong ground motion records were obtained from [27]. These records are surface records and scaled to horizontal elastic design spectra generated as per [26], through spectral matching. Thereafter, 1D site response analyses were performed on these scaled ground motion records which matched elastic design horizontal spectrum. Therefore, bedrock input motions were created for soil-structure interaction analysis. This procedure was adopted from [35]. 1D equivalent-linear site response analyses were performed on STRATA program [36]. The 1D site response

Table 2 - The soil properties on which the earthquake recording stations were built

Station Type	Soil Type	Upper and lower depths of layers (m)	Thickness (m)	Weight per unit of volume (kN/m^3)	Shear wave velocity (m/s)	Damping ratio (%)
LINC station	Top soil (organic, silty)	0-0.3	0.3	15.7	150	5
	Yellow clay (stiff)	0.3-4.59	4.29	17.66	220	3
	Brown compact gravel (dense)	4.59-5.50	0.91	18.64	300	1
	Loose thin gravel	5.50-9.80	4.30	19.62	250	2
	Large sandy brown gravel	9.80-10.70	0.90	19.62	300	1
	Yellow clay-bound gravel	10.70-11.30	0.60	19.62	250	2
	Loose brown gravel	11.30-13.40	2.10	19.62	280	2
	Red sandy gravel (dense, older)	13.40-38.70	25.30	20.60	500	1
	Bedrock	-	-	25.50	2500	1
Kashiwazaki station	Holocene dune sand (loose sand)	0-3.3	3.3	18	125	5
	Holocene dune sand (medium dense)	3.3-7	3.7	19	220	5
	Pleistocene sand (old dune sad)	7.0-12.7	5.7	20	270	5
	Pleistocene clay	12.7-17	4.3	17	215	5
	Pleistocene sandy clay	17-20.5	3.5	17	250	5
	Bedrock	-	-	21	400	5
Newhall Fire Sta	Layer 1	0-6	6	17.66	186.75	2.5
	Layer 2	6-12	6	17.66	230.04	2.5
	Layer 3	12-15.5	3.5	17.66	277.94	2.5
	Layer 4	15.5-27	11.5	17.66	308.06	2.5
	Layer 5	27-35	8	19.13	550.06	1.5
	Layer 6	35-54	19	19.62	677.60	1.5
	Layer 7	54-90	36	20.60	750.07	1.5
	Bedrock	-	-	22.56	1300	1

analysis assumes that soil deposits are horizontally layered [37]. Therefore, 1D equivalent-linear analyses were conducted in this study.

The properties of the soil strata beneath the LINC station were obtained from [38]. In [38], although only soil types and soil depths exist, shear wave velocity, weight per unit of volume and damping ratio for the soil beneath LINC station were adopted from resemble soil data in literature [39, 40, 41, 42]. The properties of the soil strata beneath the Kashiwazaki station were obtained from [43]. The properties of soil strata beneath the Newhall Fire Station were obtained from [44].

Table 2 shows the soil profiles down to bedrock. $V_{S,30}$ values in field which recorded of each of the earthquake records were presented in Table 5.

2.3. Lead Rubber Bearing

In this study, the lead rubber bearing designated HM080X3R obtained from the Bridgestone Seismic Isolation Product Range catalog [45] was selected for analysis. LRB was considered

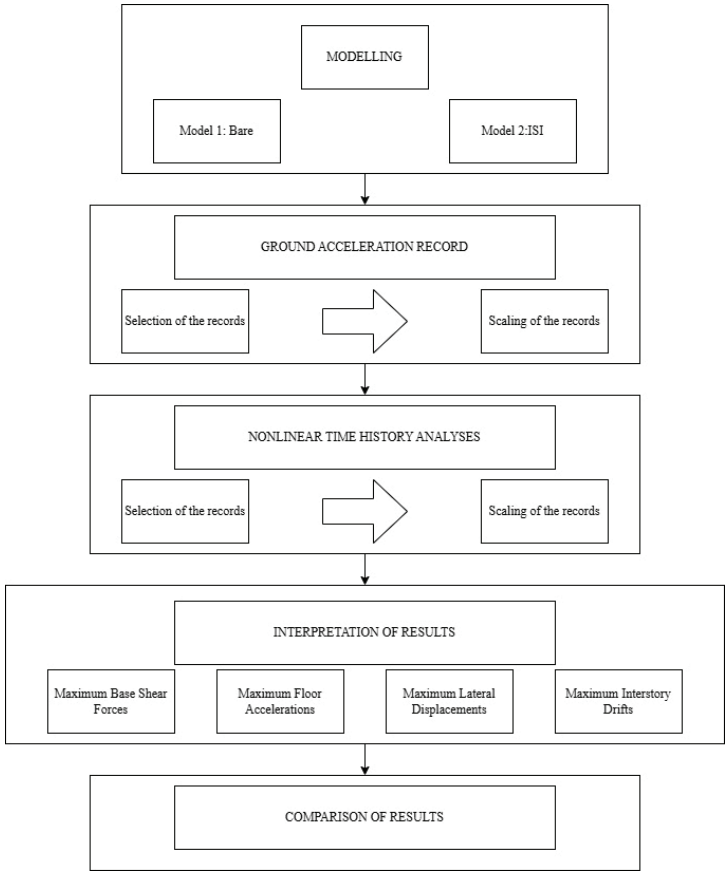

Figure 3 - Flow chart.

a link element in modelling, and the structural behavior under the selected acceleration records was calculated using the method recommended in [26] Section 14. Mechanical properties of the lead rubber bearings utilized in analyses were presented in Section 0. In addition, the optimization of these isolators was presented in Section 0.

Within the scope of the study, three distinct 3D finite element models were created. The flow chart of the method is shown in Figure 3.

3. CASE STUDY

Within the scope of this study, a seven-story reinforced concrete building was designed as a sample building. Three different models were established considering the bare structure, DD-1 nominal, and DD-2 nominal cases.

3.1. Building Information and Modelling Process

The RC building analyzed in this study consists of seven floors. The substructure height is 4.2374 m, the lead rubber bearing height is 0.2626 m, the height of each story of the superstructure is 3 m. The total height of the structure is 19.5 m. The structure has 6 axes in the X direction, and it has 11 axes in the Y direction. The spacing of every axis is 2.5 m. Concrete grade is C30/37. Rebar grade is B420C. Beam dimensions are 0.3x0.4 meters. Column dimensions of superstructure are 0.5x0.3 meters. Column dimensions of substructure are 0.75x0.75 meters. The slab thickness of superstructure is 0.1 m. The slab thickness of the substructure is 0.5 m. The structure is framed system. The structure is founded on a raft foundation. Thickness of raft foundation is 1 meter. The slab is exposed to dead load (1.6 kN/m^2), and live load (2 kN/m^2). The formwork plans of the structure and modelling are shown in Figure 4.

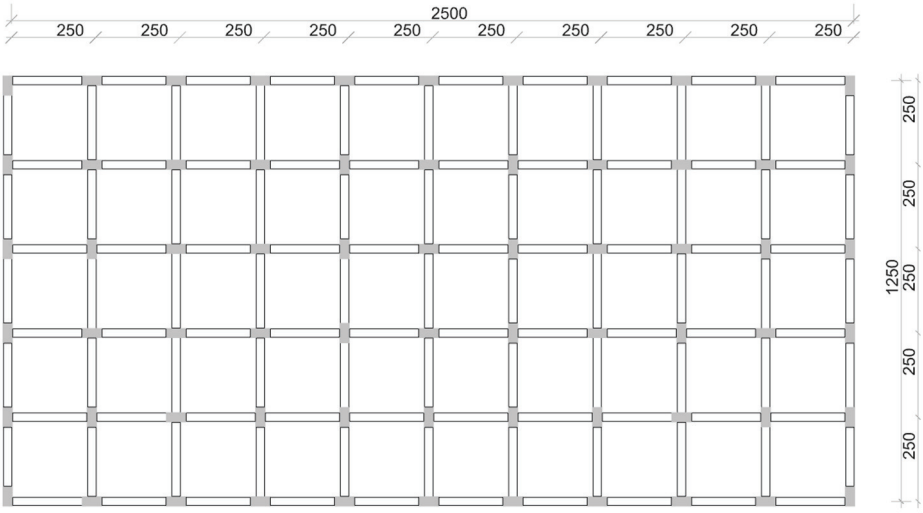

(a)

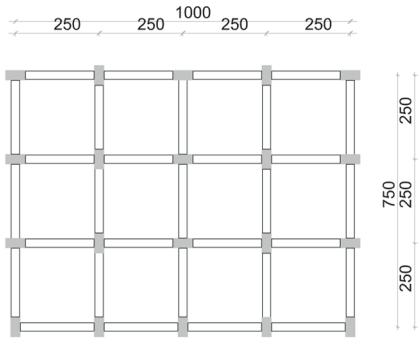

(b)

Figure 4 - Plans of the building: (a) Normal floor plan, (b) Roof floor plan.

Material properties used in the structure are given in Table 3. Earthquake parameters of the structure are given in Table 4. These parameters indicate the seismicity of the region. Design spectra can be generated by these parameters, or the performance target can be determined. Soil was modelled as eight-node finite elements. The depth, width and length of the soil are 30 m, 58.5 m and 115 m, respectively. SSI is considered in the time history analyses in this manner.

Table 3 - Material properties

Material	Grade	Weight Per Unit of Volume (kN/m^3)	Elastic Modulus (kN/m^2)	Shear Modulus (kN/m^2)	Poisson Ratio	Yield Strength (kN/m^2)	Failure Strength (kN/m^2)
Concrete	C30/37	25	33000000	13750000	0.2	-	-
Rebar	B420C	78.5	200000000	-	-	420000	483000
						Shear Wave Velocity (m/s)	**Cohesion (kN/m^2)**
Soil	ZD	21	390000	150000	0.3	264.66	30

Shear wave velocity was calculated by Eq. (2).

In Table 4, CD denotes controlled damage, UU denotes uninterrupted usage, DBD denotes displacement-based design and SBD denotes strength-based design. These performance targets are specified in [26].

The bare model and the inter-story isolated model were presented in Figure 5. Although these models were developed with a soil-structure interaction model, they were presented in that way to make them more apparent.

Table 4 - Earthquake parameters belong to the structure [26]

Parameters	Bare		Seismic isolated	
	DD-1	DD-2	DD-1	DD-2
Load-bearing system behavior coefficient (R)	8	8	1	1.2
Strength Excess Factor (D)	3	3	1	1.2
Building Significance Coefficient	1.5	1.5	1	1
Building Usage Grade (BKS)	1	1	1	1
Earthquake Design Grade (DTS)	1a	1a	1a	1a
Building Height Grade (BYS)	5	5	5	5
Performance Targets and Assessment/Design Approaches	-	CD-SBD	UU-SBD	UU-DBD-SBD

	DD-1	DD-2
SS (Coefficient of map acceleration for short period)	2.172	1.064
SDS (Coefficient of design acceleration for short period	2.172	1.14
S1 (Coefficient of map acceleration for 1 second period)	0.591	0.276
SD1 (Coefficient of design acceleration for 1 second period)	1.01	0.565
TA (s)	0.093	0.099
TB (s)	0.465	0.4945
Latitude	36.19117	
Longitude	36.1343	

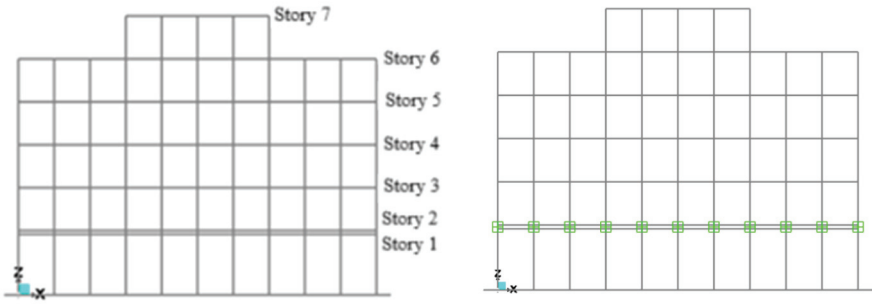

(a) (b)

Figure 5 - (a) Bare building model (b) Inter-story isolated model.

SSI model of the building is shown in Figure 6. The structure is positioned at the center of the soil system. To assign a viscous boundary condition to the interaction interface, 1-dimensional damper-exponential links were used. Horizontal elastic design spectra, shown in Figure 7, were constructed according to DD-1 (maximum credible earthquake) and DD-2 (design basis earthquake). It is based on data acquired from Türkiye Earthquake Hazard Map. However, spectral matching was performed only with the horizontal elastic design spectra

on horizontal components of the earthquake records, because it was not required that vertical components must be matched to the vertical elastic design spectrum.

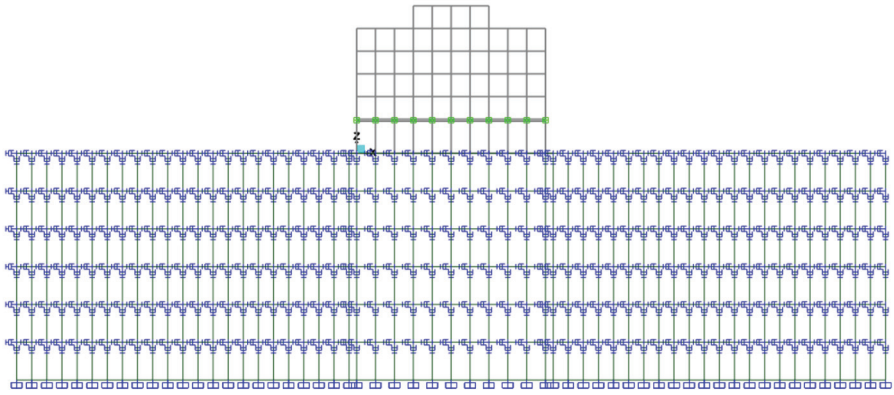

Figure 6 - Soil-structure interaction model.

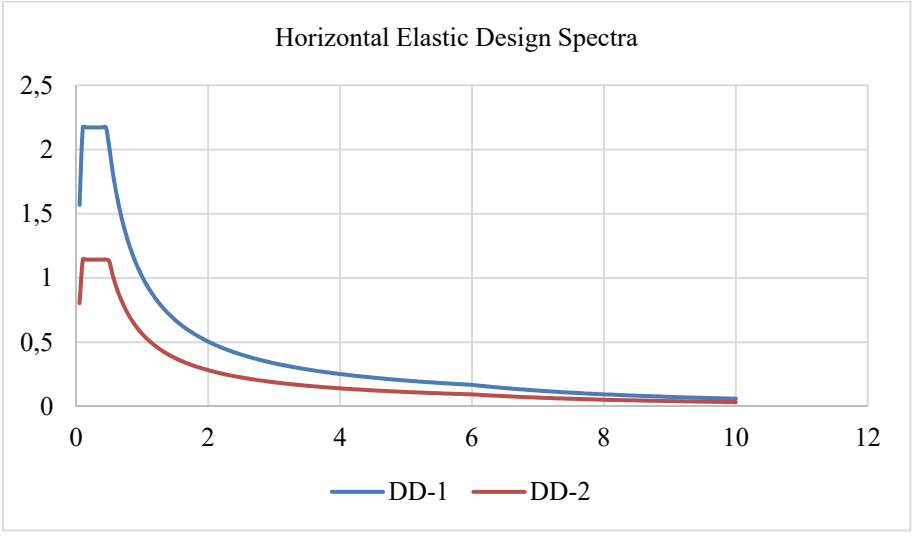

Figure 7 - Horizontal elastic design spectra based on [26].

The spectra in Figure 7 show spectral acceleration which the structure will undergo as a function of the period of structure. Acceleration records used in nonlinear dynamic analyses (time history analyses) were received from PEER [27]. Spectral matching was performed in SAP2000. Analyses were carried out using these records. In spectral matching, these records and spectra which were obtained from the AFAD Turkey Earthquake Hazard website were matched. Spectral matching was performed as specified in [26]. Information about these earthquake records is given in Table 5.

Table 5 - Information on earthquake acceleration raw records [27]

RSN	Earthquake	Station	Magnitude	$V_{S,30}$ (m/s)	Components	PGA (g)	Station Latitude	Station Longitude	Time step (s)
8102	Christchurch (CHR)	LINC	6.2	263.2	N23E	0.160458	-43.6248°	172.4679°	0.005
					N67W	0.087705			
					UP	0.09618			
4895	Chuetsu-oki(CHU)	Kashiwazaki	6.8	265.5	EW	1.249487	37.4367°	138.6017°	0.01
					NS	0.983961			
					UD	0.544417			
6927	Darfield (DAR)	LINC	7.0	263.2	N23E	0.461347	-43.6248°	172.4679°	0.005
					N67W	0.387577			
					UP	0.914513			
1044	Northridge-01 (NOR)	Newhall-Fire Sta	6.69	269.14	90	0.582989	34.387°	-118.533°	0.02
					360	0.590411			
					UP	0.54821			

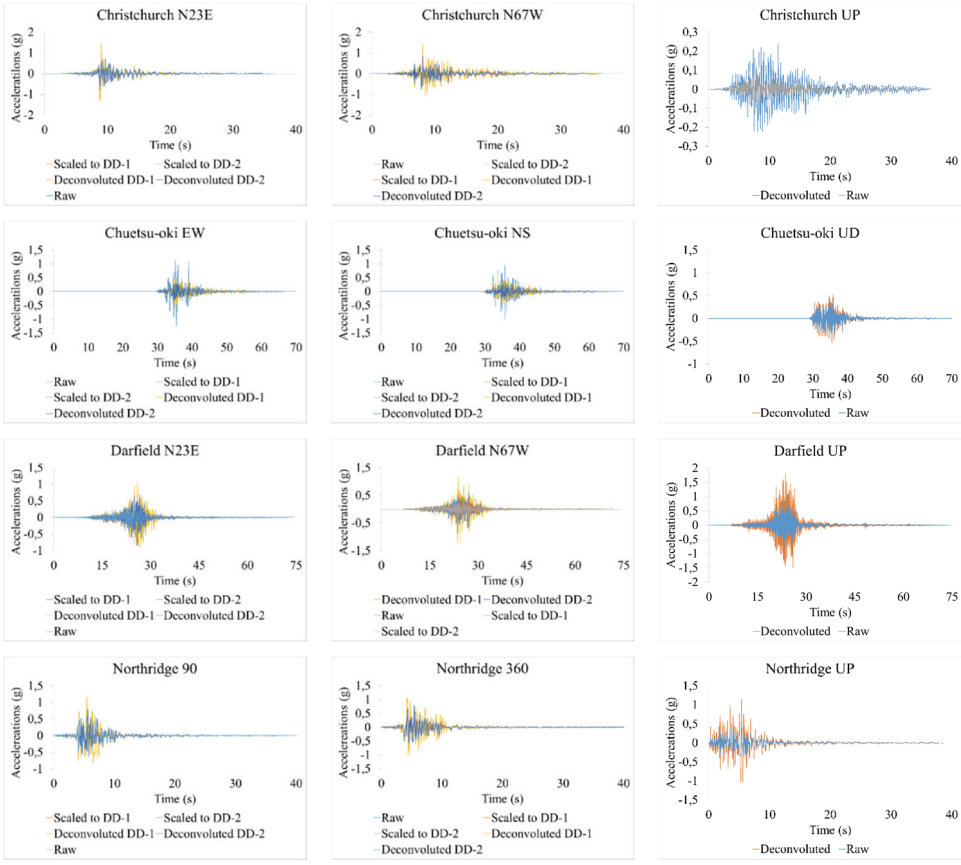

Figure 8 - Earthquake horizontal and vertical acceleration records.

Earthquake acceleration records used in time history analyses are presented in Figure 8. These records are raw and scaled. Condition 1 represents scaling of earthquake acceleration records according to the DD-1 horizontal elastic design spectrum, while Condition 2 represents the scaling according to the DD-2 horizontal elastic design spectrum. However, because the vertical components of these records were not scaled to any spectrum, the raw version of this component and corresponding deconvoluted data are presented in Figure 8.

As an initial step, DEAD LOAD+0.3*LIVE LOAD+0.3*earthquake vertical component was used in nonlinear time history analyses. However, because the vertical period of isolated building models is more than 0.1 s, the vertical components of earthquake records were used in the initial step of nonlinear time history analyses [26].

3.2. Mechanical Properties of Lead Rubber Bearing Used in Analyses

The mechanical properties of the LRB in this study are presented in Table 6. Optimization of these lead rubber bearings is described in Section 0.

Table 6 - Mechanical characteristics of Lead Rubber Bearing

B(mm) (Isolator outer diameter)	800
B_L (mm) (Isolator inner diameter)	20
G_v (Mpa) (Shear modulus of rubber material)	0.6
Total height (mm)	262.6
t (mm) (Rubber layer thickness)	6.8
Rubber layer number	23
T_r (mm) (Total rubber thickness)	156.4
A_r (mm^2) (Surface area of each of rubber layer which sticks to steel plate)	502340.66
S (shape factor)	29.39
E_0 (Mpa) (elasticity modulus)	1.2
k	0.6
E_c (Mpa) (Pressure modulus)	1245.32
K (Mpa) (bulk modulus)	2000
E_v (Mpa) (vertical rigidity modulus)	767.45
k_v (N/mm) (vertical stiffness)	2464986.2
Total bearing number	66
Mass of single lead rubber bearing (t)	0.64
Total rubber bearing mass (t)	42.24
Mass of superstructure +isolator (t)	1771.89

In Table 6, A_r, S, E_0, E_c, E_V, k_V was calculated using Eqs. (5)-(6). These equations exist in [26].

$$A_r = \left(\frac{\pi}{4}\right)(B^2 - B_L^2),\ S = \frac{(B^2 - B_L^2)}{4Bt},\ E_0 = 4G_v \tag{5}$$

$$E_c = \mathrm{E}_0(1 + 2kS^2),\ E_V = \frac{1}{\frac{1}{E_C} + \frac{1}{K}},\ k_V = \frac{E_V A_r}{T_r} \tag{6}$$

3.3. Optimization of Inter-Story Isolation

The lead rubber bearing used in the nonlinear time history analyses was selected from Bridgestone [45]. However, dynamic parameters of the aforementioned rubber bearing were optimized based on building properties, the DD-1 and the DD-2 spectral acceleration coefficients and the upper, nominal and lower bounds. These upper bound and lower bound values are used to account for temperature and environmental effects on rubber bearings, implicitly. These values and formulas are presented in Eq. (7) and (8). These formulas are based on the methodology described in [26].

$$\lambda_{upper} = \left[1 + 0{,}75\left(\lambda_{ae,upper} - 1\right)\right]\lambda_{test,upper}\lambda_{spec,upper} \tag{7}$$

$$\lambda_{lower} = \left[1 - 0{,}75\left(1 - \lambda_{ae,lower}\right)\right]\lambda_{test,lower}\lambda_{spec,lower} \tag{8}$$

Upper- and lower-bound coefficients of λ_{ae}, λ_{test}, and λ_{spec} are presented in Table 7.

Table 7 - Upper bound and lower bound values

	F_Q		k_2	
	Lower	Upper	Lower	Upper
λ_{ae}	1	1.3	1	1.4
λ_{test}	0.7	1.3	0.9	1.3
λ_{spec}	0.85	1.15	0.85	1.15
λ_{upper}	1.831375		1.9435	
λ_{lower}	0.595		0.765	

These optimized parameters of the lead rubber bearing are presented in Table 8. In this table, $F_{Q,\,lower}$, $F_{Q,\,upper}$, $k_{2,\,upper}$ and $k_{2,\,lower}$ values were obtained by multiplying the nominal values with upper- and lower-bound values presented in Table 7. This procedure was adopted from [46].

In Table 8, F_Q represents characteristic strength, k_2 represents post-elastic stiffness, k_1 represents pre-elastic stiffness, D_y represents yield displacement, F_y represents yield strength, F represents horizontal force corresponding to D displacement, k_e represents effective

Table 8 - Optimized parameters of abovementioned lead rubber bearing

	DD-1				DD-2		
	Lower	Nominal	Upper		Lower	Nominal	Upper
F_Q (kN)	24.99	42	76.91775	F_Q (kN)	24.99	42	76.91775
k_2 (kN/m)	737.1303241	963.5690511	1872.696	k_2 (kN/m)	737.1303241	963.5690511	1872.696451
k_1 (kN/m)	7371.303241	9635.690511	18726.96	k_1 (kN/m)	7371.303241	9635.690511	18726.96451
D_{target} (m)	0.369	0.272	0.168	D_{target} (m)	0.156	0.1075	0.064
D_y (m)	0.00376686	0.004843106	0.004564	D_y (m)	0.00376686	0.004843106	0.004563696
F_y (kN)	27.76666667	46.66666667	85.46417	F_y (kN)	27.76666667	46.66666667	85.46416667
F (kN)	296.9910896	304.0907819	391.5308	F (kN)	139.9823306	145.583673	196.7703229
k_e (kN/m)	804.8539013	1117.980816	2330.54	k_e (kN/m)	897.3226318	1354.266726	3074.536295
W_D (kNm)	36.50870468	44.88235826	50.28461	W_D (kNm)	15.21722468	17.24635826	18.28682719
β_e	0.05302086	0.086362189	0.121669	β_e	0.110906696	0.175386596	0.231110097
η_M	0.985229515	0.856353384	0.763228	η_D	0.788338872	0.666094669	0.596433155
T_M (s)	1.147540281	0.973664398	0.67437	T_D (s)	1.08680632	0.884655867	0.587133221
D_M (m)	0.368756086	0.271954439	0.167875	D_D (m)	0.156389803	0.107560709	0.063920736
ω_b (rad/s)	5.475350547	6.453132435	9.31712	ω_b (rad/s)	5.781329379	7.102406193	10.70146448
c_b (kN*s/m)	1028.787849	1974.973828	4017.25	c_b (kN*s/m)	2272.231656	4414.373047	8764.542701
$D_{(TM-X)}$ (m)	0.390881451	0.288271706	0.177948	$D_{(TD-X)}$ (m)	0.165773191	0.114014351	0.06775598
$D_{(TM-Y)}$ (m)	0.457257547	0.337223505	0.208165	$D_{(TD-Y)}$ (m)	0.193923355	0.133375279	0.079261712
D_{TM} (m)	0.457257547	0.337223505	0.208165	D_{TD} (m)	0.193923355	0.133375279	0.079261712

stiffness, W_D represents the area under the hysteresis curve resulting from a cycle, β_e represents damping ratio, η_M and η_D represent damping scaling coefficient, T_M and T_D represent building effective period, D_M and D_D represent horizontal displacement of rubber bearing, ω_b represents circular frequency, c_b represents damping coefficient, D_{TM} and D_{TD} represent total horizontal displacements taking into account torsion. Some of these notations were presented on the hysteresis curve of the rubber bearing in Figure 9.

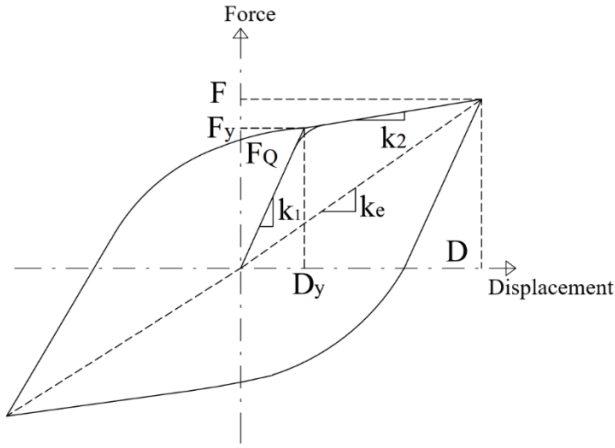

Figure 9 - Hysteresis curve of rubber bearing [26].

To perform this aforementioned optimization, required formulae are presented between Eqs. (9)-(12) [26, 47].

$$k_2 = G_V \frac{A_r}{T_r},\ D_y = \frac{F_Q}{k_1 - k_2},\ F_y = F_Q + k_2 D_y,\ F = F_y + k_2\left(D - \frac{F_y}{k_1}\right) \tag{9}$$

$$W_D = 4F_Q\left(D - D_y\right),\ k_e = \frac{F}{D},\ \beta_e = \frac{W_D}{2\pi F D},\ c_b = 2m_t\omega_b\beta_e \tag{10}$$

$$\eta_M = \sqrt{\frac{10}{5+\beta_e}},\ T_M = 2\pi\sqrt{\frac{W}{gK_M}},\ D_M = 1{,}3\left(\frac{g}{4\pi^2}\right)T_M^2\eta_M S_{ae}^{DD-1}(T_M) \tag{11}$$

$$D_{TM} = D_M\left[1 + y\frac{12e}{b^2+d^2}\right] \tag{12}$$

In Eq. (10), m_t represents the combined mass of the superstructure and the isolator, ω_b represents circular frequency. In Eqs. (11)-(12), the M index represents DD-1 (MCE). However, similar calculations can be done for DD-2 (DBE) earthquake ground motion level. The only difference is the use of DD-2 spectrum data. The hysteresis curves established based on optimization parameters are presented in Figure 10. The study by Namous et al [48] was utilized in order to establish these curves.

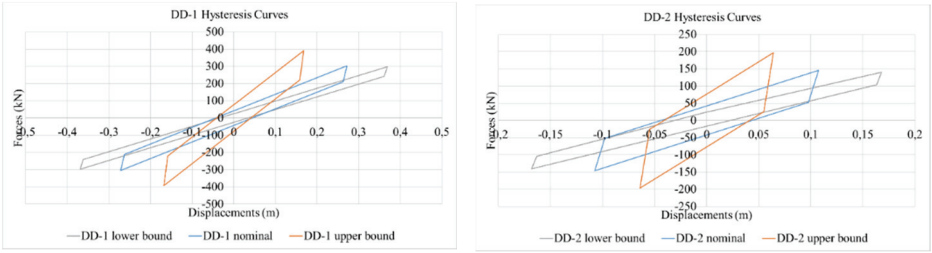

(a) (b)

Figure 10 - Hysteresis curves (a) based on DD-1 optimization parameters (b) based on DD-2 optimization parameters.

Although bearing properties were optimized based on the upper and lower bounds, only the nominal bearings were utilized in the analyses.

Rayleigh damping was chosen to calculate the building's damping. The Rayleigh damping mass and stiffness coefficients of three different building models are presented in Table 9.

Table 9 - Rayleigh damping coefficients

Structure Modelling	α	β	T_1 (s)	T_2 (s)
Bare	0.823	0.003	0.39	0.37
DD-1 nominal	0.3074	0.008	1.026	1.018
DD-2 nominal	0.3346	0.00747	0.944	0.934

In Table 9, α and β values were calculated from Eq.(13) [49]. Rayleigh damping assumes that damping is a linear combination of mass and stiffness.

$$\alpha = \xi \frac{2\omega_i\omega_j}{\omega_i+\omega_j} \quad \beta = \xi \frac{2}{\omega_i+\omega_j} \tag{13}$$

In Eq.(13), ω_i and ω_j are circular frequencies of first and second modes of the building models, respectively. In this case, the formula of the damping coefficient is given as follows:

$$C = \alpha M + \beta K \tag{14}$$

In Eq.(14), M and K are the mass and stiffness of the system, respectively.

4. RESULTS AND DISCUSSION

The study considered two different structural models, which were analyzed using all three components of four different earthquake ground motions using the nonlinear time-history (dynamic) method. A total of twelve ground-motion records were considered at two different scales (Figure 8). All analyses were repeated in two perpendicular directions (X and Y) for each building model. The results were interpreted in terms of maximum base shear force, maximum floor accelerations, lateral displacements and inter-story drifts. Because rubber bearings are not effective for the vertical component of earthquake motion, the vertical components of obtained values were ignored. In the figure legends, Bare denotes the bare model and ISI denotes the inter-story isolated building model. DD-1 denotes earthquake records scaled to the DD-1 spectrum and DD-2 denotes earthquake records scaled to the DD-2 spectrum. The X direction denotes results obtained when nonlinear time history analyses were applied in the X direction to the building models and Y direction denotes results obtained when nonlinear time history analyses were applied in the Y direction.

4.1. Examination of the Maximum Base Shear Forces

Graphical representations of the maximum base shear values obtained from nonlinear time history analyses applied to the Bare and ISI models are presented in Figure 11. Moreover, the percentage-change graph of these values is presented in Figure *12*. In the Christchurch and Darfield earthquake, since they have angular components, both the X- and Y-direction values are presented separately.

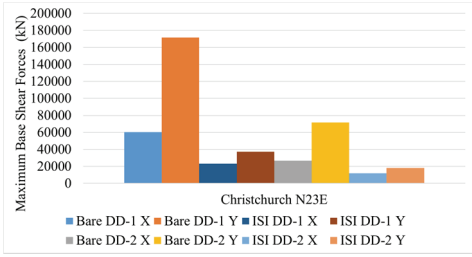

(a)

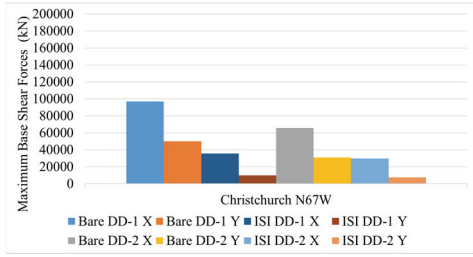

(b)

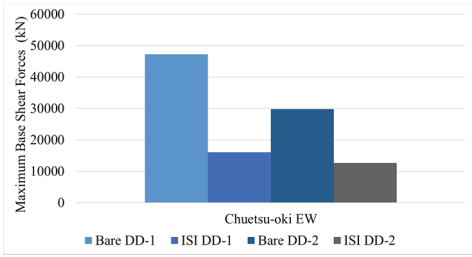

(c)

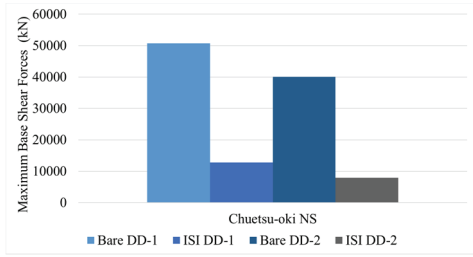

(d)

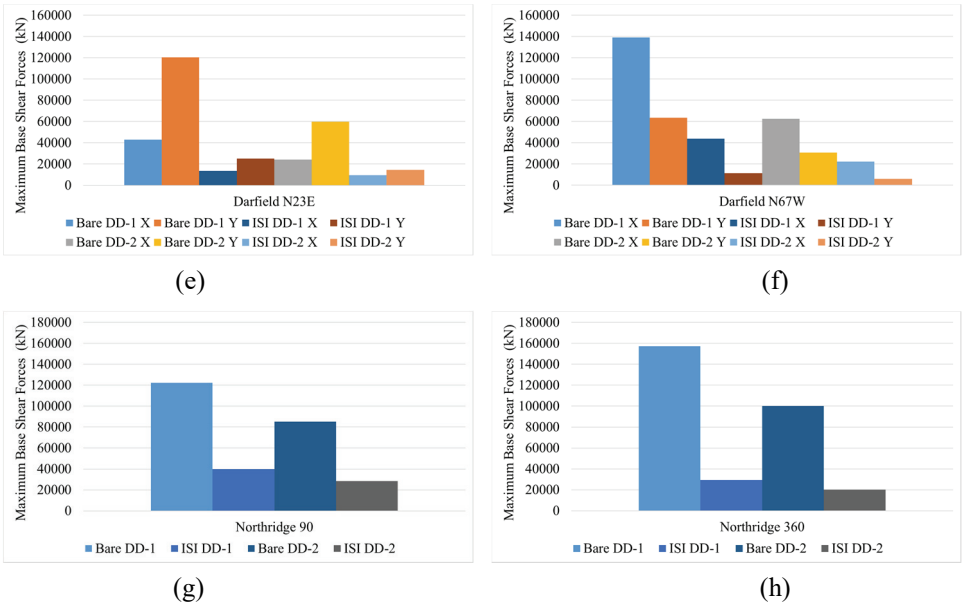

Figure 11 - Maximum base shear forces (a) Obtained data from Christchurch N23E earthquake (b) Obtained data from Christchurch N67W earthquake (c) Obtained data from Chuetsu-oki EW earthquake (d) Obtained data from Chuetsu-oki NS earthquake (e) Obtained data from Darfield N23E earthquake (f) Obtained data from Darfield N67W earthquake (g) Obtained data Northridge 90 earthquake (h) Obtained data Northridge 360 earthquake.

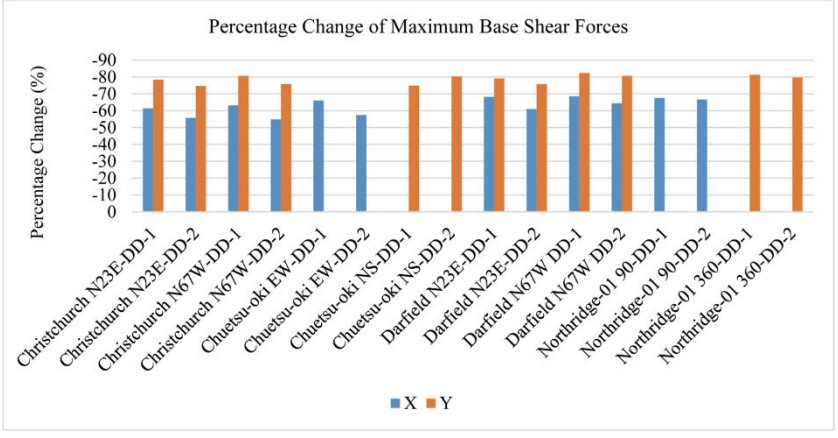

Figure 12 - Percentage changes of maximum base shear forces via inter-story isolation system according to results of bare model obtained from nonlinear time history analyses.

As seen in Figure 11, inter-story isolation reduced base shear forces in all earthquakes. Additionally, as seen in Figure *12*, more reduction in the Y direction was observed than the

X direction. The highest peak was recorded for the Northridge 360° DD-1 earthquake, with a value of 157,277.58 kN. The greatest reduction was observed for the Darfield N67W DD-1 earthquake, amounting to 82.31%. Likewise, Gao et al [20] studied a base-fixed structure, a mid-story-isolated structure, and a double-story-isolated structure while considering SSI. The study concluded that the base-fixed structure produced a greater base shear then the mid-story-isolated structure and double-story-isolated structures. Yanık and Topaloğlu [23] studied a fixed base structure, a base-isolated structure and base- and mid-story-isolated structure, while considering soil-structure interaction. The study concluded that base-and mid-story-isolated structure produced a lower base shear than the fixed-base structure.

4.2. Examination of the Maximum Floor Accelerations

Graphical representations of the maximum floor acceleration values obtained from nonlinear time history analyses applied to Bare and ISI model were presented in Figure 13. Since Christchurch and Darfield earthquakes have angular components, both X directional values and Y directional values were presented individually.

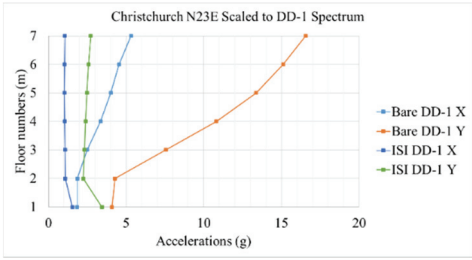

(a)

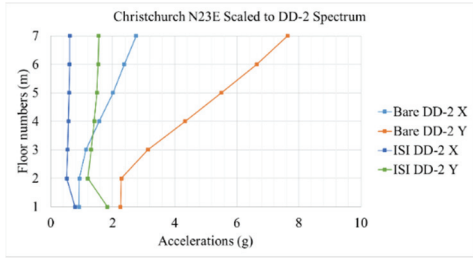

(b)

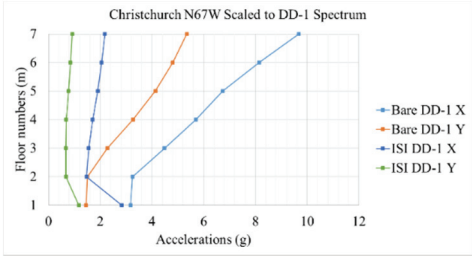

(c)

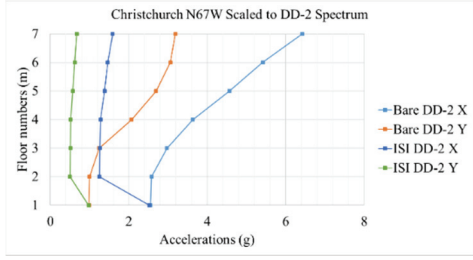

(d)

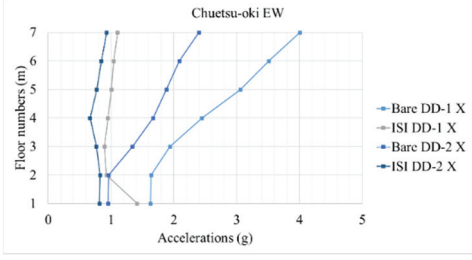

(e)

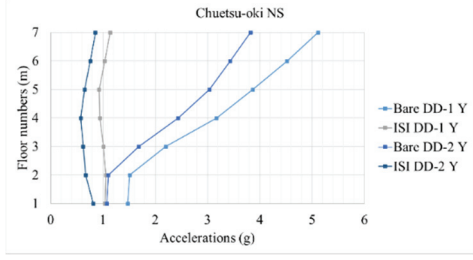

(f)

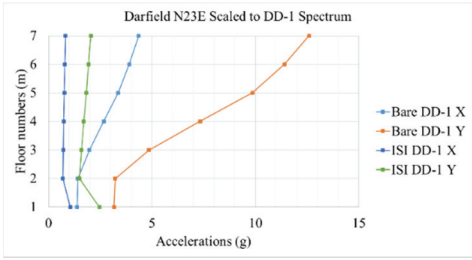

(g)

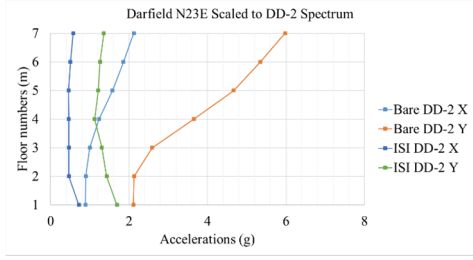

(h)

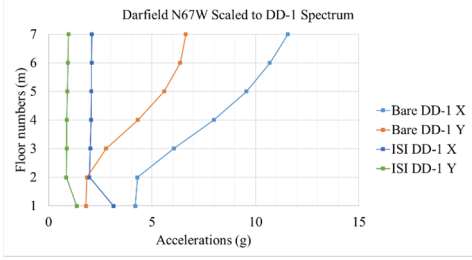

(i)

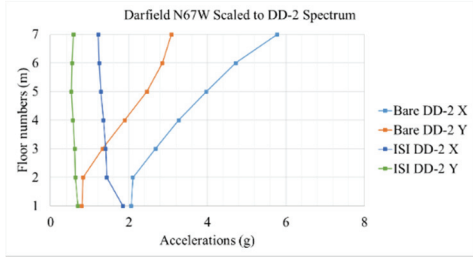

(j)

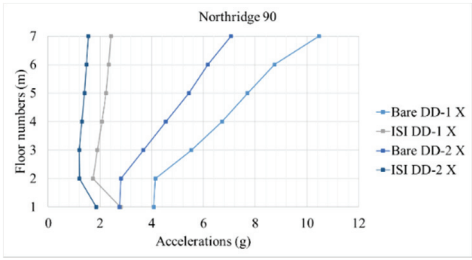

(k)

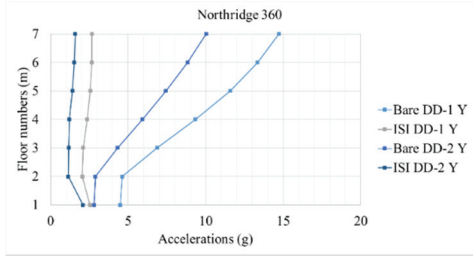

(l)

Figure 13 - Maximum floor accelerations (a) Obtained data from Christchurch N23E earthquake scaled to DD-1 spectrum (b) Obtained data from Christchurch N23E earthquake scaled to DD-2 spectrum (c) Obtained data from Christchurch N67W earthquake scaled to DD-1 spectrum (d) Obtained data from Christchurch N67W earthquake scaled to DD-2 spectrum (e) Obtained data from Chuetsu-oki EW earthquake (f) Obtained data from Chuetsu-oki NS earthquake (g) Obtained data from Darfield N23E earthquake scaled to DD-1 spectrum (h) Obtained data from Darfield N23E earthquake scaled to DD-2 spectrum (ı) Obtained data from Darfield N67W earthquake scaled to DD-1 spectrum (j) Obtained data from Darfield N67W earthquake scaled to DD-2 spectrum (k) Obtained data from Northridge 90 earthquake (l) Obtained data from Northridge 360 earthquake.

As seen in Figure 13, inter-story isolation reduced maximum floor accelerations significantly. As a result of the analyses, inter-story isolation significantly reduced top-floor accelerations. The results revealed that the highest floor acceleration was 16.56 g for the bare model;

however, when the inter-story isolation was applied, values reduced to the range of 0.67-3.44 g at the DD-1 earthquake ground motion level and 0.46-2.52 g at the DD-2 earthquake ground motion level. For example, the top-floor acceleration was reduced from 5.32 g to 1.06 g in the X direction and from 16.56 g to 2.72 g in the Y direction, respectively, when the inter-story isolation was applied. Likewise, Yanık and Topaloğlu [23] concluded that mid-story isolation was able to reduce floor accelerations, with a reduction of average 11%, while considering soil-structure interaction.

4.3. Examination of the Maximum Lateral Displacements

Graphical representations of maximum floor displacements obtained from nonlinear time history analyses were presented in Figure 14. However, in order that more area has not been covered, just one graphical representation of each earthquake amongst all component data set were represented in Figure 14.

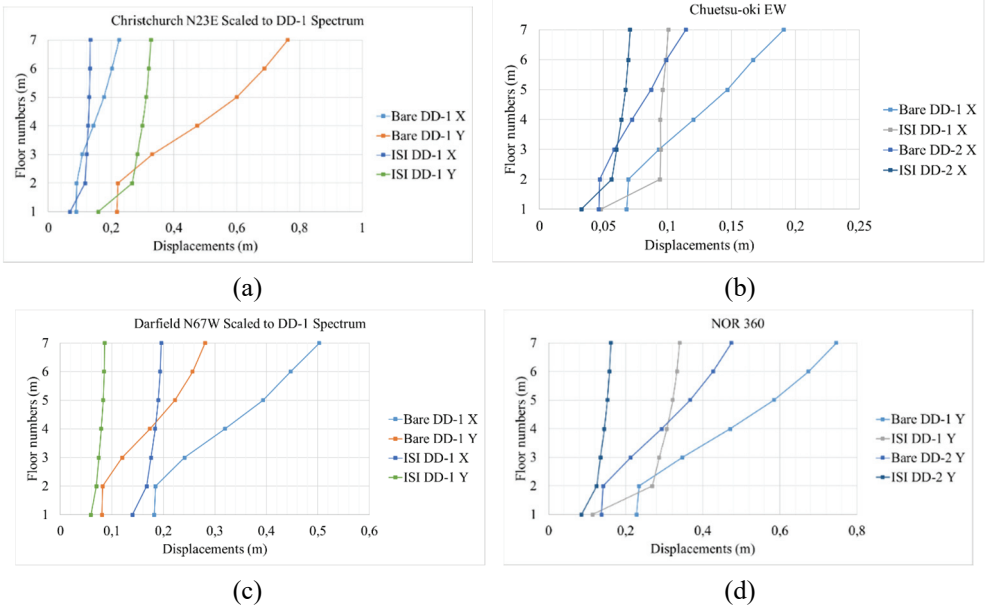

Figure 14 - Maximum lateral displacements (a) Obtained data from Christchurch N23E earthquake scaled to DD-1 spectrum (b) Obtained data from Chuetsu-oki EW earthquake (c) Obtained data from Darfield N67W earthquake scaled to DD-1 spectrum (d) Obtained data from Northridge 360 earthquake.

As seen in Table 8, the DD-1 nominal and DD-2 nominal target displacements are 0.272 and 0.1075 m, respectively. The target displacement is maximum displacement expected to occur while shifting smoothly [50].

For the bare model, the study revealed that the highest displacement values were 0.503 m and 0.762 m in the X direction at Darfield N67W DD-1 and in the Y direction at Christchurch N23E DD-1, respectively. When the inter-story isolation was applied, top-floor

displacements were found as follows: Christchurch N23E DD-1 – 0.13 m (X) and 0.326 m (Y), Chuetsu-oki EW DD-1 - 0.10 m and Chuetsu-oki EW DD-2 - 0.07 m; Darfield N67W DD-1 - 0.20 m (X) and 0.09 m (Y); Northridge 360 DD-1 - 0.34 m and Northridge 360 DD-2 0.16 m. Likewise, Gautam et al [51], Forcellini and Kalfas [52] proved that inter-story isolation can reduce maximum horizontal floor displacements.

4.4. Examination of the Maximum Inter-Story Drifts

Graphical representations of maximum inter-story drifts occurring on floors obtained from nonlinear time history analyses were presented in Figure 15. However, since [26] wants to use DD-2 earthquake ground motion level in superstructure design, only graphical representations of obtained data set from nonlinear time history analyses scaled to DD-2 spectrum were presented in Figure 15.

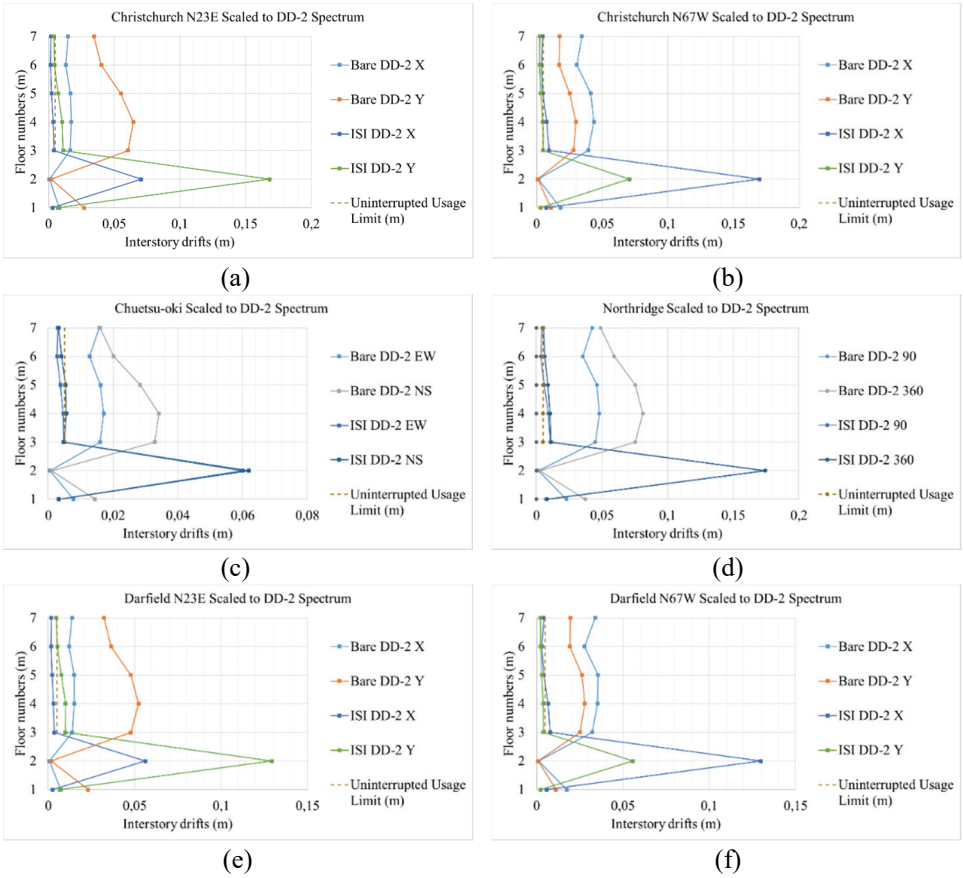

Figure 15 - Inter-story Drifts (a) Obtained data from Christchurch N23E Scaled to DD-2 Spectrum (b) Obtained data from Christchurch N67W Scaled to DD-2 Spectrum (c) Obtained data from Chuetsu-oki Scaled to DD-2 Spectrum (d) Obtained data from Northridge Scaled to DD-2 Spectrum (e) Obtained data from Darfield N23E Scaled to DD-2 Spectrum (f) Obtained data from Darfield N67W Scaled to DD-2 Spectrum.

As seen in Figure 15, inter-story isolation significantly reduced inter-story drifts, and, in general, responses in the superstructure remained within the uninterrupted usage limit. For DD-2 scaling, reductions in superstructure displacements were reported in the following ranges: Christchurch N23E - 74–89% (in all directions), Christchurch N67W - 68–85% (in all directions), Chuetsu-oki EW - 70–82%; Chuetsu-oki NS 79–86%, Darfield N23E 75–88% (in all directions), Darfield N67W 75–89% (in all directions), Northridge 90 76–91% and Northridge 360 - 85–90%. Kim and Kang [53], Khajehdezfuly et al [54] proved that inter-story isolation can lead to reduced inter-story drifts. Zhou et al [55] determined the maximum inter-story drift angles of both bare and mid-story-isolated structures considering soil-structure interaction. As a result of the analyses conducted, while maximum inter-story drift angle of the bare structure was found to be 0.0041 rad, whereas that of the mid-story-isolated structure was found to be below 0.001 rad. Additionally, Gao et al [20] observed lower inter-story drifts for the mid-story-isolated structure than in the base-fixed structure, and observed the maximum inter-story drift in isolation layer of the mid-story-isolated structure. In this study, the authors found that mid-story isolation suppressed the effects of soil-structure interaction.

5. CONCLUSIONS

Within the scope of this study, an inter-story isolation system was developed to improve the earthquake performance of a six-story reinforced-concrete structure. First, the inter-story isolation system was optimized based on building properties and elastic spectral acceleration coefficients for DD-1 and DD-2. Each model was subjected to nonlinear dynamic analysis using all components of four different earthquake ground-motion records. As a result of these analyses, the maximum base shear forces, maximum floor displacements, maximum floor accelerations, and inter-story drifts were compared. The results obtained from the nonlinear dynamic analyses of the building models are summarized as follows:

- The characteristics of the earthquake directly affect the performance of the inter-story isolation system. This condition is reflected in building's reactions.

- The inter-story isolation system significantly reduced the maximum base shear forces of bare system. Thus, when the inter-story isolation system was added, the stress on the superstructure was lower than that on bare system.

- The inter-story isolation system significantly reduced maximum floor accelerations. Also, maximum accelerations became approximately equal with the aid of inter-story isolation system, even though soil-structure interaction system was considered.

- The inter-story isolation system reduced inter-story drifts of superstructure to a large extent. Thus, inter-story drifts of superstructure were approximately equal when the inter-story isolation system was applied, even when soil-structure interaction was considered.

6. SUGGESTIONS

This study was considered under a limited set of parameters. If the number of dampers or their parameters are altered, the study results may vary significantly. Future studies could:

Evaluate the performance of ISI and FVDs using a broader range of seismic records, including near-fault ground motions.

Incorporate more complex soil models to capture site-specific effects on soil-structure interaction.

Investigate the impact of different optimization strategies for the damping system.

References

[1] Robinson, W.H. and L.R. Greenbank, *An extrusion energy absorber suitable for the protection of structures during an earthquake.* Earthquake Engineering & Structural Dynamics. **4**(3): p. 251-259. (1976). https://doi.org/10.1002/eqe.4290040306

[2] Zhang, W., C. Zhang, L. Su, Y. Zheng, and X. Du, *Experimental study on the dynamic performance of a winding rope fluid viscous damper.* Engineering Structures. **281**: p. 115786. (2023). https://doi.org/10.1016/j.engstruct.2023.115786

[3] Faiella, D. and E. Mele, *Insights into inter-story isolation design through the analysis of two case studies.* Engineering Structures. **215**: p. 110660. (2020). https://doi.org/10.1016/j.engstruct.2020.110660

[4] Charmpis, D.C., M.C. Phocas, and P. Komodromos, *Optimized retrofit of multi-storey buildings using seismic isolation at various elevations: assessment for several earthquake excitations.* Bulletin of Earthquake Engineering. **13**(9): p. 2745-2768. (2015). https://doi.org/10.1007/s10518-015-9737-y

[5] Dewen, L., Y. Fan, X.U. Jingran, L.I. Zhiang, Y. Yutong, and L.I.U. Yang, *Seismic response research of SSI effect on inter-story isolated structure.* JOURNAL OF BUILDING STRUCTURES. **43**(S1): p. 232-238. (2022). https://doi.org/10.14006/j.jzjgxb.2022.S1.0025

[6] Topaloglu, H. and A. Yanik, *Soil-structure interaction in a base and mid-story seismically isolated building.* Materials Today: Proceedings. **85**: p. 43-46. (2023). https://doi.org/10.1016/j.matpr.2023.05.253

[7] Al-Ghazali, A.S. and H. Shariatmadar, *Hybrid active control of adjacent buildings interconnected by viscous dampers utilizing type-2 fuzzy controller considering soil-structure interaction.* Structures. **33**: p. 292-306. (2021). https://doi.org/10.1016/j.istruc.2021.03.117

[8] Wilson, E.L., I. Farhoomand, and K.J. Bathe, *Nonlinear dynamic analysis of complex structures.* **1**(3): p. 241-252. (1972). https://doi.org/10.1002/eqe.4290010305

[9] Gurbuz, A. and M. Tekin, *Developing damage estimation methods for different types of reinforced concrete buildings.* (2017). https://doi.org/10.18400/tekderg.334196

[10] Rodríguez, C.A., Á.M. Rodríguez Pérez, R. López, and J.J. Caparrós Mancera, *Comparative Analysis and Evaluation of Seismic Response in Structures: Perspectives from Non-Linear Dynamic Analysis to Pushover Analysis.* **14**(6): p. 2504. (2024). https://doi.org/10.3390/app14062504

[11] Wan, F., W. Zhou, D. Liu, Y. Huo, H. Li, X. Luo, and S. Yao, *Seismic response of a stilted mid–story isolated structure in mountainous areas based on variable parameters soil–structure–interaction effect.* Structures. **51**: p. 707-717. (2023). https://doi.org/10.1016/j.istruc.2023.03.072

[12] Scarfone, R., M. Morigi, and R. Conti, *Assessment of dynamic soil-structure interaction effects for tall buildings: A 3D numerical approach.* Soil Dynamics and Earthquake Engineering. **128**: p. 105864. (2020). https://doi.org/10.1016/j.soildyn.2019.105864

[13] Tonyali, Z. and S. Ates, *The coupling finite-boundary element method for soil-structure interaction under spatially varying ground motion.* Journal of Structural Engineering & Applied Mechanics. **1**(1): p. 6-21. (2018). https://doi.org/10.31462/jseam.2018.01006021

[14] Boksmati, J.I., G.S. Madabhushi, and I.N. Thusyanthan, *Dynamic soil-structure interaction of a shallow founded shear frame and a frame equipped with viscous dampers under seismic loading.* Engineering Structures. **227**: p. 111388. (2021). https://doi.org/10.1016/j.engstruct.2020.111388

[15] Xu, L., J. Shi, Y. Wu, and Y. Lin, *Interlayer Isolation Structures Considering Soil-Structure Interaction under Long-Period Ground Motions: An Experimental Analysis.* Applied Sciences. **13**(16). (2023). https://doi.org/10.3390/app13169090

[16] Tsai, C.-S., Y.-M. Wang, and H.-C. Su, *Soil-structure interaction, damping and higher mode effects on the response of a mid-story-isolated structure founded on multiple soil layers.* International Journal of Organizational Innovation. **11**(3): p. 135. (2019).

[17] Yingxiong, W., Z. Zewei, Y.A.N. Guiyun, W.U. Zhenxiang, C. Baochun, and L.I.U. Ning, *Shaking table test of pile-soil inter-story isolated structure under far-field long-period ground motion.* JOURNAL OF BUILDING STRUCTURES. **42**(12): p. 11-22. (2021). https://doi.org/10.14006/j.jzjgxb.2020.0474

[18] Dewen, L., Y. Fan, X.U. Jingran, L.I. Zhiang, Y. Yutong, and L.I.U. Yang, *Seismic response research of SSI effect on inter-story isolated structure.* JOURNAL OF BUILDING STRUCTURES. **43**((S1)): p. 232-238. (2022). https://doi.org/10.14006/j.jzjgxb.2022.S1.0025

[19] Liu, D., L. Li, Y. Zhang, L. Chen, F. Wan, and F. Yang, *Study on seismic response of a new staggered story isolated structure considering SSI effect.* Journal of Civil Engineering Management. **28**(5): p. 397–407-397–407. (2022). https://doi.org/10.3846/jcem.2022.16825

[20] Gao, L., D. Liu, M. Lei, Y. Ding, and S. Mu, *Study on Shock-Absorbing Effect of a Double-Story Isolation Structure Considering Soil–Structure Interaction.* **13**(11): p. 2677. (2023). https://doi.org/10.3390/buildings13112677

[21] Wan, F., C. Li, H. Li, D. Liu, S. Yao, and M. Lei, *Seismic response of a mid-story-isolated structure considering soil–Structure interaction in sloping ground under three-dimensional earthquakes.* **10**. (2023). https://doi.org/10.3389/feart.2022.1098711

[22] Xiao, S., C. Li, D. Liu, W. Sun, and M. Lei, *Research on irregular plane mid story isolation structures in castor earthquake prone areas considering SSI effect.* Frontiers in Earth Science. **11**: p. 1207110. (2023). https://doi.org/10.3389/feart.2023.1207110

[23] Yanık, A. and H. Topaloğlu, *Simple Soil Effect Analysis in a Base and Mid-Story Isolated 15 Story Building.* El-Cezeri. **10**(3): p. 452-463. (2023). https://doi.org/10.31202/ecjse.1230014

[24] Wan, F., S. Qin, D. Liu, T. Zhao, Y. Zheng, H. Shan, Z. Li, F. Peng, J. Xu, and M. Lei, *Seismic response of a mid-story isolated structure considering SSI in mountainous areas under long-period earthquakes.* Earthquake Engineering Engineering Vibration. **23**(1): p. 151-161. (2024). https://doi.org/10.1007/s11803-024-2231-2

[25] Yang, Z., D. Liu, T. Ban, Y. Zhao, R. Sun, and W. Sun, *Seismic response analysis of cliff-attached isolated structures considering SSI effect under long-period ground motion in the far field.* (2024). https://doi.org/10.21203/rs.3.rs-4200850/v1

[26] TBEC, (2018). *Turkey Building Earthquake Code: Specifications for Building Design Under Earthquake Effects.*https://www.resmigazete.gov.tr/eskiler/2018/03/20180318M1-2-1.pdf

[27] University of California, B. *NGA-West2 Database*. Pacific Earthquake Engineering Research Center 2024; Available from: https://ngawest2.berkeley.edu

[28] Kramer, S.L., *Geotechnical earthquake engineering*. Pearson Education India. (1996). 8131707180

[29] Güllü, H. and F. Özel, *Microtremor measurements and 3D dynamic soil–structure interaction analysis for a historical masonry arch bridge under the effects of near- and far-fault earthquakes.* Environmental Earth Sciences. **79**(13): p. 338. (2020). https://doi.org/10.1007/s12665-020-09086-0

[30] Shahbazi, S., M. Khatibinia, I. Mansouri, and J. Hu, *Seismic evaluation of special steel moment frames undergoing near-field earthquakes with forward directivity by considering soil-structure interaction effects.* Scientia Iranica. **27**: p. 2264-2282. (2020). https://doi.org/10.24200/sci.2018.50241.1594

[31] Enelund, M. and P. Olsson, *Damping described by fading memory—analysis and application to fractional derivative models.* International Journal of Solids and Structures. **36**(7): p. 939-970. (1999). https://doi.org/10.1016/S0020-7683(97)00339-9

[32] Accaino, F., F. Da Col, G. Böhm, S. Picotti, M. Giorgi, F. Meneghini, and A. Schleifer, *Petro-physical Characterization of the Shallow Sediments in a Coastal Area in NE Italy from the Integration of Active Seismic and Resistivity Data.* Surveys in Geophysics. **44**(4): p. 1211-1238. (2023). https://doi.org/10.1007/s10712-023-09776-x

[33] Flinchum, B.A., D. Grana, B.J. Carr, N. Ravichandran, B. Eppinger, and W.S. Holbrook, *Low Vp/Vs Values as an Indicator for Fractures in the Critical Zone.* Geophysical Research Letters. **51**(2): p. e2023GL105946. (2024). https://doi.org/10.1029/2023GL105946

[34] Xie, Y., S. Chi, and M. Wang, *Influence of Variable Rigidity Design of Piled Raft Foundation on Seismic Performance of Buildings.* Mathematical Problems in Engineering. **2020**: p. 1780197. (2020). https://doi.org/10.1155/2020/1780197

[35] Kamal, M. and M. Inel (2021). *Correlation between Ground Motion Parameters and Displacement Demands of Mid-Rise RC Buildings on Soft Soils Considering Soil-Structure-Interaction*. Buildings, 2021. **11**, DOI: https://doi.org/10.3390/buildings11030125.

[36] Kottke, A.R. and E.M. Rathje, *Technical manual for Strata*. Pacific Earthquake Engineering Research Center Berkeley, California. (2009).

[37] Totani, F. (2025). *VS Profile Inversion in Heterogeneous Granular Soil Deposits: Implications for Structural Design in a Study Site (Italy)*. Applied Sciences, 2025. **15**, DOI: 10.3390/app15095032.

[38] Environment, C. *M36/1249 Well Card (Environment Canterbury)*. Environment Canterbury Well Search; Available from: https://www.ecan.govt.nz/data/well-search/printwellcard/M36_1249

[39] Stolte, A., L. Wotherspoon, B. Cox, C. Wood, S. Jeong, and J. Munro, *The influence of multiple impedance contrasts on mHVSR site period estimates in the Canterbury Plains of New Zealand and implications for site classification.* Earthquake Spectra. **39**(1): p. 288-309. (2023). https://doi.org/10.1177/87552930221130762

[40] Wair, B.R., J.T. DeJong, and T. Shantz, *Guidelines for estimation of shear wave velocity profiles*. Pacific Earthquake Engineering Research Center. (2012).

[41] Wotherspoon, L.M., R.P. Orense, B.A. Bradley, B.R. Cox, C.M. Wood, and R.A. Green, *Soil profile characterisation of Christchurch Central Business District strong motion stations.* Bulletin of the New Zealand Society for Earthquake Engineering. **48**(3): p. 146-156. (2015). https://doi.org/10.5459/bnzsee.48.3.146-156

[42] Darendeli, M.B., K.H. Stokoe, R.B. Gilbert, F.Y. Menq, and W.K. Choi, *Development of a new family of normalized modulus reduction and material damping curves*. The university of Texas at Austin. (2001). 0493366970

[43] Yoshida, N., H. Goto, K. Wakamatsu, S. Aoi, S. Fukumoto, and T. Mikami, *Investigation on Record at K-NET Kashiwazaki during the 2007 Niigataken-chuetsu-oki earthquake.* http://www.civil.tohokugakuin.ac.jp/yoshida/inform/chuetsuoki/k-net-e.pdf. (2007).

[44] Lavallée, D., R.J. Archuleta, and P.-C. Liu, *Modeling and Estimates of Nonlinear Effects in Strong Earthquake Motion for the Los Angeles Area*. Institute for Crustal Studies, University of California, Santa Barbara. (2002). https://earthquake.usgs.gov/cfusion/external_grants/reports/01HQGR0049.pdf

[45] Bridgestone, (2022). Seismic Isolation Product Line Up, Bridgestone https://www.bridgestone.com/products/diversified/antiseismic_rubber/pdf/catalog_201710.pdf

[46] Ye, K., Y. Xiao, and L. Hu, *A direct displacement-based design procedure for base-isolated building structures with lead rubber bearings (LRBs).* Engineering Structures. **197**: p. 109402. (2019). https://doi.org/10.1016/j.engstruct.2019.109402

[47] Karimi, M.R.B. and M.C. Genes, *Effectiveness of FVD-BIS for protecting a base-isolated high-rise building against resonance.* Earthquakes Structures. **21**(4): p. 351-370. (2021). https://doi.org/10.12989/eas.2021.21.4.351

[48] Namous, R., T. El Korany, T. Khalifa, and S. Elkhoraby, *Seismic Response of Seismic Isolated Structures subject to Near Fault &Far Fault Ground Motions.* Journal of Engineering Research. **6**. (2022). http://dx.doi.org/10.21608/erjeng.2022.166478.1103

[49] Chen, X., J. Duan, and Y. Li, *Mass proportional damping in nonlinear time-history analysis*. in *3rd International Conference on Material, Mechanical and Manufacturing Engineering (IC3ME 2015)*. 2015. Atlantis Press. 567-571 https://doi.org/10.2991/ic3me-15.2015.112

[50] Cardone, D., P. G., and M. and Dolce, *Direct Displacement-Based Design of Buildings with Different Seismic Isolation Systems.* Journal of Earthquake Engineering. **14**(2): p. 163-191. (2010). https://doi.org/10.1080/13632460903086036

[51] Gautam, R., G.B. Motra, and P.N. Maskey, *Performance of Elastomeric Base Isolated Medium-Rise Reinforced Concrete Building in High Seismic Region*. in *Proceedings of 14th IOE Graduate Conference*. 2023. Nepal. 798-807

[52] Forcellini, D. and K.N. Kalfas, *Inter-story seismic isolation for high-rise buildings.* Engineering Structures. **275**: p. 115175. (2023). https://doi.org/10.1016/j.engstruct.2022.115175

[53] Kim, H.-S. and J.-W. Kang, *Optimal Design of Smart Mid-Story Isolated Control System for a High-Rise Building.* International Journal of Steel Structures. **19**(6): p. 1988-1995. (2019). https://doi.org/10.1007/s13296-019-00258-8

[54] Khajehdezfuly, A., Y.M. Younus, A. Khademalrasoul, and A. Al-Mubarak, *Dynamic Response of Inter-story Isolated High-rise Building Subjected to Wind Flow.* Iranian Journal of Science and Technology, Transactions of Civil Engineering. **48**(6): p. 4307-4331. (2024). https://doi.org/10.1007/s40996-024-01410-z

[55] Zhou, W., X. Li, C. Huang, and F. Wang, *Study of Split-Foundation Structural Response with Application of Mid-Story Isolation Techniques Under Soil-Structure Interaction.* Journal of Earthquake Engineering. **29**(9): p. 1870-1893. (2025). https://doi.org/10.1080/13632469.2025.2487872